Measurement of Magnetic Moment at the Atomic Scale in a High T_C Molecular Based Magnet

M.-A. Arrio,*,† Ph. Sainctavit,†,‡ Ch. Cartier dit Moulin,‡ Ch. Brouder,‡,§ F. M. F. de Groot,‡ T. Mallah,⊥ and M. Verdaguer⊥

Laboratoire de Minéralogie-Cristallographie, CNRS URA9, Universités Paris VI et VII, 4 place Jussieu, 75252 Paris Cedex 05, France; Laboratoire pour l'Utilisation du Rayonnement Electromagnétique, Bât. 209d, CNRS-CEA-MEN, 91405 Orsay Cedex, France; Laboratoire de Physique du Solide de Nancy, CNRS URA 155, BP239, 54506 Vandœuvre-lès-Nancy, France; and Laboratoire de Chimie des Métaux de Transition, CNRS URA419, Université Paris VI, 4 place Jussieu, 75252 Paris, France

The molecular-based magnet $Cs^I[Ni^{II}Cr^{III}(CN)_6]\cdot 2H_2O$ is a ferromagnetic with a Curie temperature $T_C = 90$ K. Its structure consists of face-centered cubic lattice of Ni^{II} ions connected by $Cr(CN)_6$ entities. We have recorded X-ray magnetic circular dichroism (XMCD) at nickel $L_{2,3}$ edges. It clearly evidences that nickel(II) is in a high-spin configuration and ferromagnetically coupled to the surrounding Cr^{III}. Through ligand field multiplet calculations, we have determined the total magnetic moment carried by Ni^{II}. Special attention has been paid to the magnetic anisotropy that complicates the calculation of the cross section for a powder. By using sum rules derived for XMCD, it has been possible to extract the orbital and spin contributions to the total magnetic moment. A somewhat too small magnetic moment is found on nickel. A complete calculation taking into account the multiplet coupling effect and the covalent hybridization allowed to determine the precise ground state of nickel and showed that hybridization cannot be responsible for the experimental low nickel magnetic moment. The origin of this effect is discussed.

Introduction

Conventional techniques in magnetism measure total magnetic moment (susceptibility measurements by SQUID, Faraday balance). Other more sophisticated techniques such as polarized neutron diffraction can give information on specific groups of atoms but measurements are only possible on large single crystals. X-ray magnetic circular dichroism (XMCD) is a new technique that has recently received strong interest by the community of magnetism. Magnetic circular dichroism has long been known in the energy range of visible light but was not investigated till recently in the X-ray range due to the lack of sources of circular polarized X-rays. The development of synchrotron radiation in the past decade impulsed the field of X-ray spectroscopies and XMCD was first observed in 1987.[1]

In the first section we present the elaboration of a molecular based magnet and its magnetic properties are reviewed. The second section is a basic summary of XMCD theory where the sum rules are discussed. The third section is dedicated to the experimental measurements, and the fourth one outlines the results concerning the magnetic properties of the magnet that have been obtained from the comparison between experiments and calculations.

Molecular-Based Magnet

We have studied $Cs^I[Ni^{II}Cr^{III}(CN)_6]\cdot 2H_2O$, a new type of magnet from inorganic chemistry. This magnet belongs to the family of bimetallic cyanides whose general formula is $Cs^I[A^{II}B^{III}(CN)_6]\cdot nH_2O$, where A and B are 3d transition metal ions. It is synthesized through soft chemistry engineering at room temperature.[2,3] A solution of cesium chloride (CsCl) is

dropped into a solution of potassium hexacyanochromate, $K_3[Cr^{III}(CN)_6]$, to get the yellow precipitate $Cs^I_2K[Cr^{III}(CN)_6]$. Then a solution of $Ni(NO_3)_2\cdot 6H_2O$ (10^{-2} mol in 300 mL) is added dropwise to a 100 mL solution containing an equimolar amount of $Cs^I_2K[Cr^{III}(CN)_6]$ that is vigorously stirred up. A light blue precipitate appears and $Cs^I[Ni^{II}Cr^{III}(CN)_6]\cdot 2H_2O$ is collected by centrifugation and then carefully washed with distilled water.

The structure of $Cs^I[Ni^{II}Cr^{III}(CN)_6]\cdot 2H_2O$ consists of a three-dimensional assembly of structural motifs $-N\equiv C-Cr-C\equiv N-Ni-$ where the metallic cations are arranged in a rock salt lattice.[2,3] The Ni^{II} ions are surrounded by six nitrogen atoms and the Cr^{III} ions by six carbon atoms. Both have an octahedral symmetry. Cesium ions are present in half of the tetrahedral sites of the structure as shown in Figure 1. Two water molecules are present per formula unit. Their location although unclear is supposed to be around the Cs^I ions. Water is always present unless the material is heated above 100 °C.

Using powder X-ray diffraction we found that the compound is pure and well crystallized.[2,3] The cell parameter is $a = 10.57$ Å. This value is consistent with data obtained from XAFS spectroscopy at nickel and chromium K-edges: EXAFS determined that the chromium−carbon distance is 2.06 Å, nickel−nitrogen distance is 2.10 Å, and the $C\equiv N$ bridge is 1.14 Å, giving a cubic cell parameter around 10.60 Å. All the peaks of the powder diffractograms can be indexed and no spurious phase is formed. From infrared spectroscopy, it can be inferred that no Ni^{II} are coordinated to carbon atoms of the cyano bridges.[4]

In $Cs^I[Ni^{II}Cr^{III}(CN)_6]\cdot 2H_2O$, an orbital interpretation based on the model of Kahn et al.[5] allows to foresee a short-range ferromagnetic interaction between the two ions. In that model, the three unpaired electrons of Cr^{III} (d^3) are described by t_{2g} orbitals partially delocalized on the π system of cyanides and particularly on p_π orbitals of the nitrogen atoms. The two
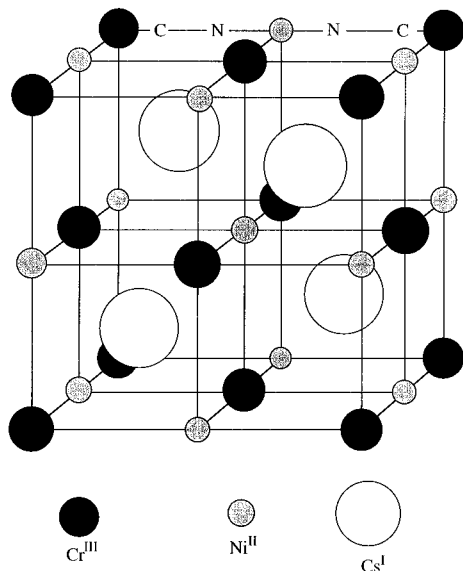
Figure 1. Crystallographic structure of $Cs^I[Ni^{II}Cr^{III}(CN)_6] \cdot 2H_2O$. Cesium atoms are in the interstitial sites and water molecules are not represented.
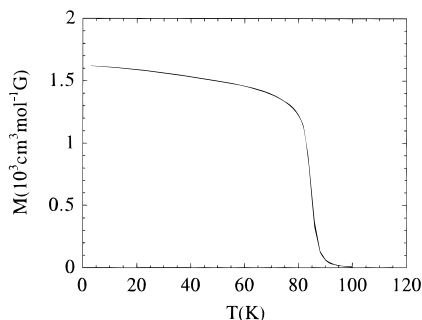

Figure 2. Magnetization at $H = 10$ G as a function of temperature. The Curie temperature is 90 K.

unpaired electrons of Ni^{II} (d^8) are described by e_g orbitals partially delocalized on the surrounding nitrogen atoms (p_σ orbitals). It results in a strict orthogonality between the two kinds of orbitals of different symmetry: t_{2g} for Cr^{III} and e_g for Ni^{II}. Furthermore, the delocalization of the t_{2g} (Cr^{III}) orbitals and the e_g (Ni^{II}) on the nitrogen atoms allows a strong overlap density $t_{2g}-e_g$ on the nitrogen atom; the large value of the bielectronic exchange integrals $\langle t_{2g}Cr(1) \cdot e_g Ni(2)|(e^2/r_{12})|t_{2g}Cr(2) \cdot e_g Ni(1)\rangle$ governs the value of the ferromagnetic short range interaction, reflected in the high Curie temperature ($T_C = 90$ K). The magnetic properties of the compound have been thoroughly measured by conventional techniques. From magnetization curves, the saturation moment at 3 T is found to be 5.2 μ_B per molecular unit at 3 K. This is consistent with the two Bohr magnetons carried by nickel and the three by chromium. This is also supported by the magnetic susceptibility measurements at high temperature. Field-cooled magnetization measurements at 10 G clearly evidence that the Curie temperature is 90 K (Figure 2). The hysteresis loop shows that the remnant magnetic moment is 1.5 μ_B per formula unit with a coercive field of 80 G: $Cs^I[Ni^{II}Cr^{III}(CN)_6] \cdot 2H_2O$ is indeed a magnet.[2]

Neutron diffraction with non spin polarized neutrons has been performed on powdered samples.[3] Diffractograms have been registered above and below the Curie temperature. The difference between the two diffractograms has been analyzed. The difference amounts to 2% of the average signal. From the absence of superstructure peaks (nickel and chromium are coupled ferromagnetically) it can be inferred that the magnetic moment carried by nickel and chromium are not much different,

leading to a value for the nickel moment somewhat higher than 2 μ_B. No refinement on the difference signal could be made because of the small number of peaks for a cubic powder and the poor quality of the signal/noise ratio.

From EPR measurements on $Cs^I[Ni^{II}Cr^{III}(CN)_6] \cdot 2H_2O$ it has been possible to determine the effective Landé factor of Ni^{II}. The EPR spectrum presents one peak that gives the averaged g factor of the nickel and chromium atoms; we found $g = 2.05$. From EPR measurements on $Zn^{II}_3[Cr^{III}(CN)_6]_2 \cdot xH_2O$, we obtained $g_{Cr} = 1.99$ in agreement with previous measurements on $[Cr(CN)_6]^{3-}$.[6] We extracted the g factor of nickel using the relation[7]

$$g_S = \frac{1+c}{2}g_1 + \frac{1-c}{2}g_2$$

with

$$c = \frac{S_1(S_1+1) - S_2(S_2+1)}{S(S+1)}$$

and we obtained $g_{Ni} = 2.15 \pm 0.02$. That value of g_{Ni} is comparable to values obtained on different nickel complexes that have been measured by EPR.[8] From effective factor g_{Ni} one can deduce that the ratio $\langle L_z \rangle / \langle S_z \rangle = 0.15 \pm 0.02$ from the application of $\langle L_z \rangle + 2\langle S_z \rangle = g_{eff}\langle S_z \rangle$. The ratio $\langle L_z \rangle / \langle S_z \rangle$ will be compared to XMCD measurements in the Results and Discussion section.

X-ray Absorption Spectroscopy and X-ray Magnetic Circular Dichroism

An XAS experiment is an atomic selective technique that measures the absorption cross section. During the absorption process the atom undergoes a transition from an initial state to a final state and when the absorption cross section is expressed in the electric dipole approximation the interaction Hamiltonian reads $\vec{\epsilon} \cdot \vec{r}$, where $\vec{\epsilon}$ is the polarization vector characterizing the photon beam.[9−13]

XMCD is performed when the cross section of a magnetic sample is registered for circularly polarized light. The XMCD signal is the difference between the two cross sections for left ($\vec{\epsilon} \cdot \vec{r} = (x + iy)/\sqrt{2}$) and right ($\vec{\epsilon} \cdot \vec{r} = (-x + iy)/\sqrt{2}$) circularly polarized light.[14]

We have measured $L_{2,3}$ edges of nickel. The main channel corresponds to a transition from the initial state $2p^6 3d^8$ to the final state $2p^5 3d^9$. The channel that corresponds to transitions toward continuum s states is ignored since it is commonly found negligible.[15] In the final state the 2p spin−orbit coupling is large and the states constructed with $J_{2p} = {}^3/_2$ lie 17.1 eV below those constructed with $J_{2p} = {}^1/_2$. The L_3 and L_2 edges are well separated, although some intermixing still exists. The $L_{2,3}$ edges correspond to transitions toward the 3d orbitals that are spin-polarized in a magnetic compound. The two effects (spin−orbit coupling and spin polarization of the 3d orbitals) make the dependence of the cross section with the photon helicity as large as 50% (or more) of the isotropic cross section. By definition, the cross sections are labeled σ_0 for linear polarization parallel to the magnetic field, σ_+ for left circular polarization, and σ_- for right circular polarization (in both circular polarization, the propagation vector is parallel to the magnetic field).

Thole and Carra et al.[16] have developed several sum rules that can be applied to XMCD spectra.[17−19] From these sum rules, it is possible to extract the average values $\langle L_z \rangle$ and $\langle S_z \rangle$, and hence also the magnetic moment $M = -\mu_B\langle L_z + 2S_z \rangle$ carried by the absorbing atom. The validity of the sum rule for $\langle L_z \rangle$ evaluation has been checked in rare-earth and 3d transition metallic or intermetallic compounds.[17−21] The validity

Magnetic Moment in a High T_C Molecular Based Magnet

J. Phys. Chem., Vol. 100, No. 11, 1996 **4681**

of the sum rule for $\langle S_z \rangle$ has still not received much confirmation from the experimental point of view.[21-26] In the case of transition metals, we follow Carra's remark by taking the magnetic dipole operator $\langle T_z \rangle \approx 0$ in eq 7 of ref 20. In the Results and Discussion section we shall explain why this approximation is justified. The two sum rules for $L_{2,3}$ edges for dipolar transitions read

$$\frac{I_{2,3}{}^+ - I_{2,3}{}^-}{I_{2,3}{}^+ + I_{2,3}{}^- + I_{2,3}{}^0} = -\frac{\langle \phi_i | L_z | \phi_i \rangle}{2(10 - n)} \quad \text{(a)}$$

and

$$\frac{(I_3{}^+ - I_3{}^-) - 2(I_2{}^+ - I_2{}^-)}{I_{2,3}{}^+ + I_{2,3}{}^- + I_{2,3}{}^0} = -\frac{2}{3(10 - n)}\Big[\langle \phi_i | S_z | \phi_i \rangle +$$

$$\frac{7}{2}\langle \phi_i | T_z | \phi_i \rangle\Big] \quad \text{(b)}$$

where n is the occupation number of the 3d orbital ($n = 8$ for Ni^{II}), $|\phi_i\rangle$ the Ni^{II} ground state, $I_3{}^+$ the integral of the absorption cross section over the L_3 edge for left-polarized photons and similar definitions for other I. The $+$, $-$, 0 indices relate respectively to left, right, linear polarization, and $I_{2,3}{}^+ = I_3{}^+ + I_2{}^+$. The I values can be computed from the experimental data ($I = \int \sigma/h\nu \, d(h\nu)$), so that direct determinations of $\langle S_z \rangle$ and $\langle L_z \rangle$ are possible from experimental data.

Measurements at Nickel $L_{2,3}$ Edges

We measured XMCD at nickel $L_{2,3}$ edges in the molecular-based magnet $Cs^I[Ni^{II}Cr^{III}(CN)_6]\cdot 2H_2O$ on the soft X-ray SU22 beamline of the storage-ring Super-ACO at LURE (Orsay). The photon source is an asymmetric wiggler that delivers a high flux of circularly polarized light above and below the orbital plane. At the nickel $L_{2,3}$ edges (850 eV) the flux is 10 times larger than the one delivered by bending magnets and amounts to 10^{12} photons/s/100 mA/mrad^2/0.1% BW. For XMCD we select the photons emitted 0.3 mrad above the orbit plane. The flux is left elliptically polarized and the averaged polarization rate before the monochromator can be calculated from the emission of the wiggler: it is 80% and constant on the whole energy range of nickel $L_{2,3}$ edges. The elliptically polarized white beam is monochromatized by a two beryl crystal monochromator described elsewhere.[27,28] The crystals are high-quality natural Ukrainian yellowish gems that have been cut along the (100) planes. The main advantage of a beryl crystal monochromator is the high resolution that can be achieved. At 850 eV, the ultimate instrumental broadening, resulting from the beam divergence and the width of the reflection profile, has been measured to be 0.25 eV.

The monochromatic beam goes through a 0.7 μm thick aluminum foil and the intensity of the photocurrent is measured to determine the flux upstream the sample: it is typically in the 1 pA range. The beam then falls on the sample cooled down to 20 K and magnetized by a superconducting magnet. A full magnetization of the sample is obtained for a magnetic field of 0.1 T at 20 K.[3] This point is deduced from SQUID measurements at high field and was checked by verifying that the XMCD signals at 20 K are the same for magnetic fields of 1 or 0.1 T. Except when specially specified, all experiments where carried out with a magnetic field of 1 T. The X-ray absorption spectra are recorded by measuring the photocurrent emitted by the sample on a 617 Keithley electrometer. For a machine current of 200 mA, the average signal below the L_3 edge is around 0.5 pA and reaches 1.5 pA at L_3 edge maximum. Great care has been taken to the elimination of any systematic noise.

For a better conductivity, the powder was pasted on a grid carved on metal sheet. A stability of 1 fA is currently achieved.

During a XMCD experiment, a first spectrum, labeled $\sigma_{\uparrow\uparrow}$, is registered with the magnetic field parallel to the propagation vector of the photons. Then a second spectrum, labeled $\sigma_{\uparrow\downarrow}$, is registered with the magnetic field antiparallel to the propagation vector of the photons. $\sigma_{\uparrow\uparrow}$ and $\sigma_{\uparrow\downarrow}$ depend on the circular polarization rate (τ) and are related to σ_+ and σ_- through $\sigma_{\uparrow\uparrow} = [(\tau + 1)/2]\sigma_+ + [(1 - \tau)/2]\sigma_-$ and $\sigma_{\uparrow\downarrow} = [(1 - \tau)/2]\sigma_+ + [(\tau + 1)/2]\sigma_-$. It can be shown that, in the electric dipole approximation, reversing the magnetic field is equivalent to changing the helicity of the beam. The XMCD signal is the difference ($\sigma_{\uparrow\downarrow} - \sigma_{\uparrow\uparrow}$) between the two spectra. Since the XMCD signal is obtained by difference between two spectra that are not registered at the same time, great care is needed in the normalization process: we checked that the two spectra registered with fully linearly polarized light for two directions of the magnetic field differ by a constant multiplication factor equal to 1.1. We used the same factor to normalize $\sigma_{\uparrow\uparrow}$ and $\sigma_{\uparrow\downarrow}$ spectra. All the experiments have also been performed above and below the orbit plane and yielded the same, although reversed, dichroic signal.

As stated above, the measurements were performed on a beam line where the photons are monochromatized by a two-crystal assembly. In such an experimental setup, the transfer of the circular polarization is far from perfect. Close to the Brewster angle (45° for X-rays) the crystals behave like polaroid and transform any type of light in almost purely linearly polarized light. In experiments at nickel $L_{2,3}$ edges, the Bragg angle varies from 62° to 67° and the depolarization is not too large. We have computed the transfer function of the crystal in the framework of the dynamical theory: the polarization rate is reduced behind the monochromator and depends on the energy. In order to extract reliable quantitative information from experimental data, the exact polarization at each energy has to be considered: 37.1% at L_3 edge (853 eV) and 30.9% at L_2 edge (870.3 eV).[29] To ascertain the determination of the polarization rate, we measured the XMCD signal of fully magnetized metallic nickel at 20 K and 1 T. The polarization rate is extracted from a comparison with ab initio calculated XMCD signal.[30] We found that the polarization rate is equal to 37 ± 4% at L_3 edge and 30 ± 3% at L_2 edge in agreement with the expected values (insert in Figure 3).

Results and Discussion

The two spectra $\sigma_{\uparrow\uparrow}$ and $\sigma_{\uparrow\downarrow}$ at nickel $L_{2,3}$ edges are plotted in Figure 3. Each spectrum is the sum of six spectra for each direction of the magnetic field, with an accumulation time of 1 s per point. Although the samples are insulating compounds and the photocurrent is low, a very good signal/noise ratio can be obtained. The spectra are normalized so that the average spectrum $^1/_2(\sigma_+ + \sigma_-)$ is equal to 1 at the maximum of L_3 edge. This procedure is repeated for any comparison of theoretical and experimental spectra in this paper. When plotting the XMCD signal (Figure 3), the experimental spectra have been renormalized to 100% of circular polarization rate and the cross sections have been divided by the energy for a direct application of the sum rules. The spectra are characteristic of Ni^{II} in the triplet state[31] as can be confirmed by the multiplet calculations. The net magnetic moment of the sample is parallel to the magnetic moment of chromium and the sign of the experimental XMCD signal proves that nickel(II) ions are indeed coupled ferromagnetically to chromium(III) ions.

The calculations are performed in the crystal field multiplet theory.[11-13,32,33] It takes exactly into account spin−orbit coupling and treats the environment of the absorbing atom
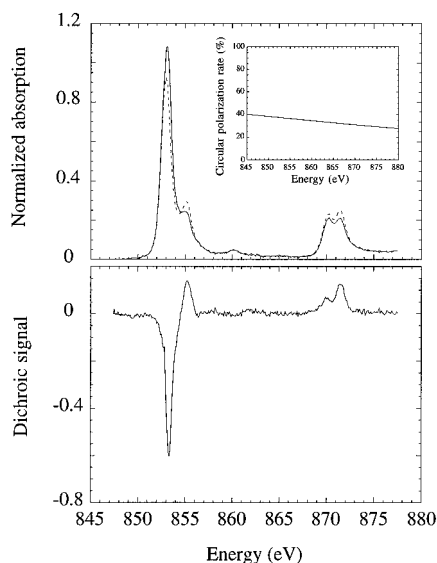
Figure 3. (Top) Experimental $\sigma_{\uparrow\uparrow}$ (line) and $\sigma_{\uparrow\downarrow}$ (dash) at nickel $L_{2,3}$ edges in $Cs^I[Ni^{II}Cr^{III}(CN)_6]\cdot 2H_2O$. (Bottom) XMCD signal $\sigma_{\uparrow\downarrow} - \sigma_{\uparrow\uparrow}$ normalized to 100% of circular polarization. The measurements are performed at 20 K and in a magnetic field of 1 T. The energy-dependent circular polarization rate is plotted in insert.

through crystal field parameters. In octahedral symmetry, the degeneracy of the 3d orbitals is lifted in two components t_{2g} and e_g. The orbitals t_{2g} and e_g are also split but in a less effective way by spin−orbit coupling and Zeeman effect. In octahedral symmetry, the crystal field strength is determined by only one parameter, the average energy separation between t_{2g} and e_g, commonly labeled $10Dq$. The parameter is determined by UV−visible electronic spectroscopy and equals to $\approx$1.3 eV around the nickel ions. In a first step we present a calculation in a single configuration where no account of nickel−nitrogen hybridization has been treated explicitly. The covalency effects, which can be responsible for the presence of additional satellites in the spectra, cannot be reproduced in this model.

The sample is a powder of crystallites with cubic crystallographic symmetry. Without magnetic field the dipolar cross sections are isotropic for any crystallites. When a magnetic field is applied, the presence of a net magnetization of the sample breaks the cubic symmetry in each crystallite. Due to magnetic anisotropy the break of cubic symmetry depends on the orientation of the magnetic field with respect to the crystallographic axes of the crystallites. To take into account this effect, the powder spectrum has to be calculated by averaging cross sections for all possible directions of magnetization with respect to the symmetry axes of the crystallites. Since the complete calculation would be intractable, we used the approximate method of integration developed by Ayant et al.[34] It states that the powder cross section can be obtained to a good approximation by a well-balanced average of cross sections calculated with particular directions of the magnetic field. In the case of cubic symmetry, the powder spectrum is given by

$$\sigma_{powder} = \frac{176}{385}\,\sigma(B||C_2) + \frac{99}{385}\,\sigma(B||C_3) + \frac{110}{385}\,\sigma(B||C_4)$$

where $\sigma(B||C_2)$, $\sigma(B||C_3)$, and $\sigma(B||C_4)$ are the cross sections corresponding to the magnetic field B parallel to the following directions: [110] or C_2, [111] or C_3, and [001] or C_4. We performed the multiplet calculations for a magnetic field parallel to C_2, C_3, and C_4. The isotropic spectra for any of the three directions are very similar as can be expected since the Zeeman Hamiltonian is a small perturbation that cannot be resolved by the experimental resolution. On the contrary, when linear or
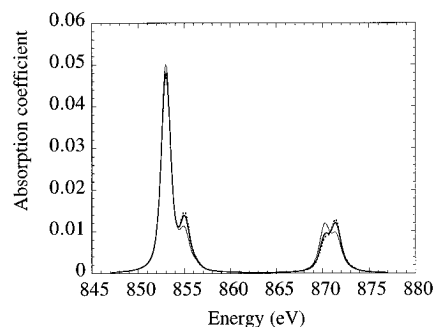

Figure 4. Ni^{II} theoretical $^1/_2(\sigma_+ + \sigma_-)$ spectra at nickel $L_{2,3}$ edges calculated with the magnetic field parallel to $C_2(110)$ (thick solid line), to $C_3(111)$ (dots), and to $C_4(100)$ (thin solid line).
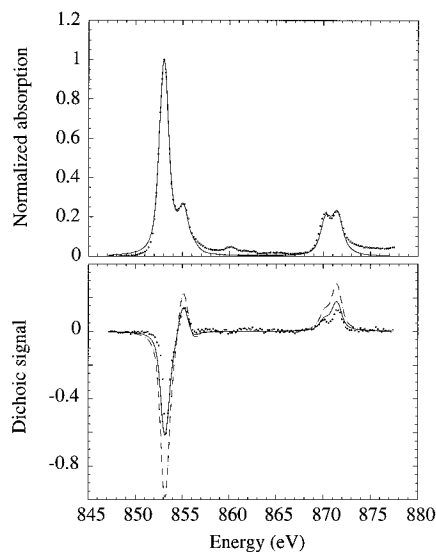

Figure 5. (Top) Experimental (dots) and theoretical (line) $^1/_2(\sigma_+ + \sigma_-)$ spectra at nickel $L_{2,3}$ edges in $Cs^I[Ni^{II}Cr^{III}(CN)_6]\cdot 2H_2O$. (Bottom) Experimental (dots), theoretical (dash), and theoretical divided by 1.6 XMCD signal renormalized to fully circular polarized light. The calculations are performed with the following parameters: $\zeta_{2p} = 11.4$ eV, $\zeta_{3d} = 0.1$ eV, $10Dq = 1.4$ eV, temperature = 0 K.

circular dichroism is calculated, some interesting differences are present due to different degeneracy lift and different dipole allowed transitions. Large differences between the average spectra $^1/_2(\sigma_+ + \sigma_-)$ for $\sigma(B||C_2)$, $\sigma(B||C_3)$, and $\sigma(B||C_4)$ can be observed in Figure 4. This proves that a well-balanced averaging procedure is essential to allow the extraction of physical quantities from the comparison between experimental and calculated $^1/_2(\sigma_+ + \sigma_-)$ spectra. Moreover X-ray magnetic circular and linear dichroism should give much information on the magnetic anisotropy, although the impossibility of growing large enough single crystals did not permit us to address experimentally this question. For the three magnetic orientations, the circular dichroic signals $\sigma_- - \sigma_+$ only differ by 3% which means that the shape of XMCD at nickel $L_{2,3}$ edges is almost insensitive to the magnetic anisotropy.

The crystal field and spin−orbit parameters are adjusted to produce the best agreement between the experimental and the powdered averaged theoretical cross section $^1/_2(\sigma_+ + \sigma_-)$. The calculation is performed at 0 K and the best agreement is obtained for spin−orbit parameters $\zeta_{2p} = 11.4$ eV and $\zeta_{3d} = 0.1$ eV, a crystal field parameter $10Dq = 1.4$ eV. The crystal field parameter is in agreement with the one obtained by optical spectroscopy.

Figure 5 compares experimental and theoretical $^1/_2(\sigma_+ + \sigma_-)$ spectra. The only difference is at 860 eV where a clearly visible feature is present on the experimental spectra and absent on the theoretical ones. This satellite is interpreted as due to

hybridization with the surrounding ligands and will be evidenced by the hybridization calculation presented below.[35,36] Despite this resonance, the overall agreement between theory and calculation is good enough to allow us to rely on the description of the ground state made in the calculations. It is then possible to extract information about the ground state. The irreducible representation of Ni^{II} ground state is Γ_5^+ when spin−orbit coupling and crystal field Hamiltonians are switched on. The Γ_5^+ nickel ground state is a pure ^3F term (99.92% of ^3F and 0.08% of ^1G and ^1D) that is made up of 52% of $^3F_{J=4}$ states, 32% of $^3F_{J=3}$ states, and 16% of $^3F_{J=2}$ states. If spin−orbit coupling is neglected, the ground state can be decoupled in pure spin and orbital parts and is given by $^3A_{2g}$. In the real case, where spin−orbit coupling exists, ^3A_g represents the main part of the actual ground state Γ_5^+.

The experimental and calculated XMCD signals are plotted in Figure 5. The shape of the experimental spectrum is well reproduced by the calculation, but its amplitude is 1.6 times smaller than the theoretical one. We applied the sum rules to the experimental XMCD spectrum. From the theoretical calculations, we found that the linear magnetic dichroic signal $[^1/_2(\sigma_+ + \sigma_-) - \sigma_0]$ is small and then $^1/_2(\sigma_+ + \sigma_-)$ is a good approximation for the isotropic spectrum ($\sigma_{iso} = ^1/_3(\sigma_+ + \sigma_- + \sigma_0) \approx ^1/_2(\sigma_+ + \sigma_-)$). The application of the sum rules (a) to the experimental spectra gives $M_L = -\langle L_z \rangle \mu_B = 0.1 \pm 0.03$ μ_B, where $\mu_B > 0$. Although the crystal field parameter is large, the orbital momentum is not completely quenched. This originates from the deviation of the ground state from the pure $^3A_{2g}$ state. As stated above, the computation of $\langle S_z \rangle$ through the spin sum rule requires the knowledge of the average value of the spherical tensor T_z. We calculated $\langle T_z \rangle$ for Ni^{II} ground state and we found $\langle T_z \rangle = 0.0017$. From the application of the spin sum rule (b) to the experimental spectra, we obtained $M_S = -2\langle S_z \rangle \mu_B = 0.78$ μ_B if we neglect $\langle T_z \rangle$ and $M_S = -2\langle S_z \rangle \mu_B = 0.80$ μ_B if we take into account $\langle T_z \rangle$. In the case of Ni^{II}, the error induced by neglecting $\langle T_z \rangle$ is not large, it is less than 3% of the total magnetic moment. The total magnetic moment on Ni^{II} is found equal to $M = -[\langle L_z \rangle + 2\langle S_z \rangle]\mu_B = 0.9$ $\mu_B \pm 0.1$ μ_B per absorbing Ni^{II} ion. The error on the determination of $\langle L_z \rangle$ and $\langle S_z \rangle$ is mainly related to the uncertainty of circular polarization rate (10%). For $\langle L_z \rangle$ it is somewhat larger than 10% because L$_2$ and L$_3$ dichroic signals tend to cancel and systematic errors can occur from normalization process. The Ni^{II} magnetic moment extracted from XMCD measurements is lower than the one (≈ 2 μ_B) expected for a fully magnetized Ni^{II} atom in $^3A_{2g}$ triplet state. The orbital and spin moments deduced from the crystal field multiplet calculation are $M_L = 0.2_8$ μ_B and $M_S = 2.0$ μ_B. We are going to show in the following that the origin of the too low value for the magnetic moment does not lie in hybridization between 3d and ligand orbitals.

A possible origin for the loss of magnetic moment could be hybridization between Ni^{II} ions and the neighboring nitrogen atoms. To take into account the hybridization effects, we performed multiplet calculations with electronic configuration interactions.[35,36] In that model, the Ni^{II} states are represented by a mixture of the two electronic configurations 3d^8 and 3d$^9\underline{L}$, where d$^9\underline{L}$ is a configuration where an extra electron coming from the ligand orbitals is added on the 3d shell; $\underline{L}$ stands for ligand hole. Figure 6 shows the theoretical $^1/_2(\sigma_+ + \sigma_-)$ cross section and theoretical XMCD signal. In that model it has been possible to reproduce the satellite at 860 eV. The fitting procedure of the experimental spectrum is more intricate than for the one configuration model. We used $\Delta = 5.3$ eV, $U_{cd} - U_{dd} = 1$ eV, $V(e_g) = 2$, and $V(t_{2g}) = -1$ (these parameters have been described by Kotani and we kept his notations[37]). We find that the Ni^{II} ground state is a mixture of 3d^8 that counts
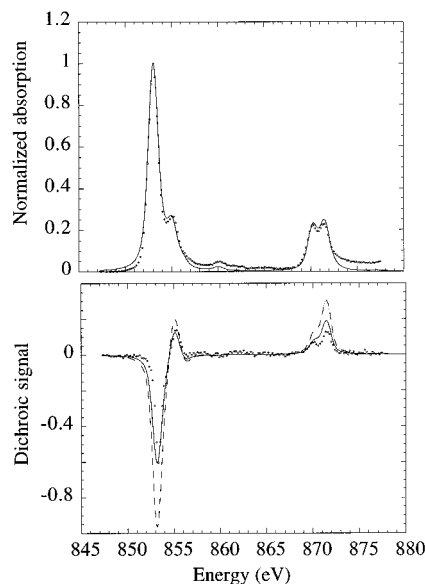

Figure 6. (Top) Experimental (dots) and theoretical (line) $^1/_2(\sigma_+ + \sigma_-)$ spectra at nickel L$_{2,3}$ edges in Cs^I[Ni^{II}Cr^{III}(CN)$_6$]·2H$_2$O. (Bottom) Experimental (dots), theoretical (dash), and theoretical divided by 1.6 XMCD signal renormalized to fully circular polarized light. The calculations are performed with hybridization (relevant parameters are given in text).

for 90% and of d$^9\underline{L}$ that counts for 10%. This result shows that Ni^{II} has a very ionic character compared to the values obtained by Kotani for a set of Ni^{II} compounds.[37] Although one would expect that the contribution from d$^9\underline{L}$ would tend to decrease M$_S$, one finds by applying the sum rules to the theoretical spectra that both M$_L$ and M$_S$ are not much affected by hybridization: taking $n = 8.1$ in expressions a and b and neglecting $\langle T_z \rangle$, we found $M_L = 0.2_7$ μ_B and $M_S = 1.8$ μ_B. The covalency tends to decrease the total magnetic moment by less than 10% ($M = 2.3$ μ_B without covalency and $M = 2.1$ μ_B with covalency). Most of this effect comes from the variation of 3d holes number between pure 3d^8 and 3d$^8 - 3$d$^9\underline{L}$ mixture.

An explanation for the low value of the XMCD Ni magnetic moment could be related to an incomplete magnetization of the nickel atoms. To check this hypothesis, we studied the effect of the applied magnetic field and the temperature on the magnetization. First, we performed at 20 K a XMCD measurement with an external magnetic field of 5 T. It was found that the XMCD signal had the same amplitude as for the 1 T experiment to less than 5% relative error. Second, we registered with a SQUID magnetometer the magnetization at saturation at 3 and 20 K. We found that the magnetization varies from 5.2 to 4.9 μ_B and that in both cases it is well reached for magnetic field lower than 0.5 T. Then one can safely consider that any bulk Ni^{II} ion has reached full magnetization in our experiments performed at 20 K with 1 T magnetic field. Nevertheless, since total electron yield detection is surface sensitive, surface nickel ions might not be feeling the exchange magnetic field or present strong magnetic anisotropy that would make the magnetization perpendicular to the surface negligible. This hypothesis cannot be discarded.

The experimental value for $\langle L_z \rangle / \langle S_z \rangle$ is $0.2_6 \pm 0.05$ and the theoretical value extracted from either crystal or ligand field multiplet calculation is around $0.2_9 \pm 0.05$. EPR measurements have shown that $\langle L_z \rangle / \langle S_z \rangle$ in Ni^{II} should be around 0.15 ± 0.02. One sees that the $\langle L_z \rangle / \langle S_z \rangle$ determination by our measurements is larger than the one determined by EPR. This effect supports the idea that Ni^{II} ions undergo a strong magnetic anisotropy and that $\langle L_z \rangle$ and $\langle S_z \rangle$ measurements do not refer to bulk magnetic Ni^{II} ions. This type of disagreement has already been

4684 *J. Phys. Chem., Vol. 100, No. 11, 1996*

Arrio et al.

mentioned by other authors who also found that $\langle L_z \rangle / \langle S_z \rangle$ extracted from XMCD is usually larger than the one extracted from other techniques. Since the orbital sum rule has been found to work reasonably well on 3d metals as nickel, cobalt, and iron, we start from the idea that the orbital sum rule works well and then $\langle L_z \rangle = -0.1$. From $\langle L_z \rangle / \langle S_z \rangle = 0.15 \pm 0.02$ one gets $\langle S_z \rangle = -0.7$ ($M_S = 1.4 \pm 0.1\ \mu_B$). In this hypothesis the total magnetic moment is then $M = 1.5 \pm 0.1\ \mu_B$. This is a reasonable value for Ni^{II} in such compound where part of the nickel moment is carried by the 4p orbitals and the neighboring nitrogen atoms. Indeed XMCD experiments performed at nickel K edge[38] have shown a strong dichroic signal evidencing that a magnetic moment is carried by the 4p orbitals. This 4p moment must be small compared to the one carried by 3d orbitals. On the other hand, XMCD measurements performed at nitrogen K edge have shown that nitrogen atoms carry a very weak magnetic moment.[39] As predicted by Figgis et al.[40] through polarized neutron diffraction experiments and local density functional calculations,[41] one expects some delocalization of the nickel magnetic moment on the six neighboring nitrogen atoms.

Conclusion

We have fully studied the nickel $L_{2,3}$ edges in the bimetallic cyanide Cs^I[Ni^{II}Cr^{III}(CN)$_6$]·2H$_2$O and have been able to evidence a strong XMCD signal on the Ni^{II} ion. The spectra were recorded at 20 K with a magnetic field produced by a superconducting magnet. We have calculated XAS and XMCD spectra in the ligand field multiplet approach and we have shown that hybridization has to be introduced for a complete simulation of the experimental spectra: even a small satellite at 860 eV is reproduced with correct intensity and energy. The 3d^{9}L̲ configuration weights for 10% in Ni^{II} ground state and tends to decrease the spin and the orbital momentum. In doing the calculations, we particularly paid attention to two important details that are usually neglected: first, the nullity of T_z was checked and can be explained from geometrical considerations and second, the averaged spectra for a powder sample were computed by taking into account the magnetic anisotropy in a cubic crystal field.

Although experimental and calculated isotropic spectra did agree very well, we have pointed out a serious discrepancy between the magnetic moment extracted from XMCD sum rules and the one that is expected for an almost pure triplet state for Ni^{II}. By comparison with EPR measurements we deduced that total electron yield measurements do not provide information on bulk magnetized ions. Surface anisotropy is responsible for the incomplete saturation of Ni^{II} ions and large $\langle L_z \rangle$ contribution relative to $\langle S_z \rangle$.

References and Notes

(1) Schütz, G.; Wagner, W.; Wilhelm, W.; Kienle, P.; Zeller, R.; Frahm, R.; Materlik, G. *Phys. Rev. Lett.* **1987**, *58*, 737−740.

(2) Gadet, V.; Mallah, T.; Castro, I.; Veillet, P.; Verdaguer, M. *J. Am. Chem. Soc.* **1992**, *114*, 9213−9214.

(3) Gadet, V. Ph.D. Thesis, University of Paris VI, 1992.

(4) Nakamoto, K. *Infra-red and Raman Spectra of Inorganic and Coordination Compounds*; Wiley Interscience: New York, 1978.

(5) Kahn, O.; Galy, O.; Journaux, Y.; Jaud, J.; Morgenstern-Badarau, I. *J. Am. Chem. Soc.* **1982**, *104*, 2165.

(6) Bowers, K. D. *Proc. R. Soc. (London)* **1952**, *A65*, 860. Baker, J. M.; Bleaney, B.; Bowers, K. D. *Proc. Phys. Soc. (London)* **1956**, *B69*, 1205.

(7) Bencini, A.; Gatteschi, D. *EPR of Exchange Coupled Systems*; Springer-Verlag: Berlin, 1990.

(8) Wertz, J. E.; Bolton, J. R. *Electron Spin Resonance - Elementary Theory and Practical Applications*; McGraw Hill Series in Advanced Chemistry; McGraw-Hill: New York, 1972.

(9) Carra, P.; Altarelli, M. *Phys. Rev. Lett.* **1990**, *64*, 1286−1288.

(10) Brouder, C.; Hikam, M. *Phys. Rev. B* **1991**, *43*, 3809−3820.

(11) van der Laan, G.; Kirkman, I. W. *J. Phys.: Condens. Matter* **1992**, *4*, 4189−4204.

(12) van der Laan, G.; Thole, B. T. *Phys. Rev. B* **1991**, *43*, 13401−13411.

(13) de Groot, F. M. F.; Fuggle, J. C.; Thole, B. T.; Sawatzky, G. A. *Phys. Rev. B* **1990**, *42*, 5459−5468.

(14) Born, M.; Wolf, E. *Principles of Optics*; Pergamon Press: London, Los Angeles, 1959.

(15) Bianconi, A.; Della Longa, S.; Li, C.; Pompa, M.; Congiu-Castellano, A.; Udron, D.; Flank, A. M.; Lagarde, P. *Phys. Rev. B* **1991**, *44*, 10126−10138.

(16) Carra, P.; König, H.; Thole, B. T.; Altarelli, M. *Physica B* **1993**, *192*, 182.

(17) Thole, T.; Carra, P.; Sette, F.; van der Laan, G. *Phys. Rev. Lett.* **1992**, *68*, 1943−1946.

(18) Altarelli, M. *Phys. Rev. B* **1993**, *47*, 597−598.

(19) Carra, P.; Thole, B. T.; Altarelli, M.; Wang, X. *Phys. Rev. Lett.* **1993**, *70*, 694−697.

(20) Schillé, J.-Ph.; Kappler, J.-P.; Sainctavit, Ph.; Cartier dit Moulin, Ch.; Brouder, Ch.; Krill, G. *Phys. Rev. B* **1993**, *48*, 9491−9496.

(21) Chen, C. T.; Idzerda, Y. U.; Lin, H. J.; Smith, N. V.; Meigs, G.; Chaban, E.; Ho, G. H.; Pellegrin, E.; Sette, F. *Phys. Rev. Lett.* **1995**, *75*, 152−155.

(22) Vogel, J.; Sacchi, M. *Phys. Rev. B* **1994**, *49*, 3230−3234.

(23) Dunn, J. H.; Arvanitis, D.; Mårtensson, N.; Tischer, M.; May, F.; Russo, M.; Baberschke, K. *J. Phys.: Condens. Matter* **1995**, *7*, 1111−1119.

(24) Samant, M. G.; Stöhr, J.; Parkin, S. S. P.; Held, G. A.; Hermsmeier, B. D.; Herman, F. *Phys. Rev. Lett.* **1994**, *72*, 1112−1115.

(25) O'Brien, W. L.; Tonner, B. P. *Phys. Rev. B* **1994**, *50*, 12672−12681.

(26) Wu, R.; Freeman, A. J. *Phys. Rev. Lett.* **1994**, *73*, 1994−1997.

(27) Sainctavit, Ph.; Lefebvre, D.; Cartier dit Moulin, Ch.; Laffon, C.; Brouder, Ch.; Krill, G.; Schillé, J.-Ph.; Kappler, J.-P.; Goulon, J. *J. Appl. Phys.* **1992**, *72*, 1985−1988.

(28) Sainctavit, Ph.; Lefebvre, D.; Arrio, M.-A.; Cartier dit Moulin, Ch.; Kappler, J.-P.; Schillé, J.-Ph.; Krill, G.; Brouder, Ch.; Mallah, T. *Jpn. J. Appl. Phys.* **1993**, *32*, 295−298.

(29) Lefebvre, D.; Sainctavit, Ph.; Malgrange, C. *Rev. Sci. Instrum.* **1994**, *65*, 2556−2561.

(30) van der Laan, G.; Thole, B. T. *J. Phys. Condens. Matter* **1992**, *4*, 4181−4188.

(31) van der Laan, G.; Thole, B. T.; Sawatzky, G. A.; Verdaguer, M. *Phys. Rev. B* **1988**, *37* (11), 6587−6589.

(32) Cowan, R. D. *The Theory of Atomic Structure and Spectra*; University of California Press: Berkeley, CA, 1981.

(33) Butler, P. H. *Point Group Symmetry, Applications, Methods and Tables*; Plenum: New York, 1991.

(34) Ayant, Y.; Belorizky, E.; Guillot, M.; Rosset, J. *J. Phys.* **1965**, *26* (7), 385−389.

(35) van der Laan, G.; Zaanen, J.; Sawatzky, G. A.; Karnatak, R.; Esteva, J.-M. *Phys. Rev. B* **1986**, *33*, 4253−4263.

(36) Sawatzky, G. A. *Core-Level Spectroscopy in Condensed Systems*; Springer-Verlag: Kashikojima, Japan, 1987; pp 99−133.

(37) Kotani, A.; Okada, K. *Tech. Rep. ISSP* **1992**, Ser. A, 2562.

(38) Verdaguer, M.; Mallah, T.; Hélary, C.; L'Hermite, F.; Sainctavit, Ph.; Arrio, M.-A.; Babel, D.; Baudelet, F.; Dartyge, E.; Fontaine, A. *Nucl. Instrum. Methods B* **1995**, *208*, 765−767.

(39) Arrio, M.-A.; Sainctavit, Ph.; Cartier dit Moulin, Ch.; Brouder, Ch.; Mallah, T.; Verdaguer, M.; Journaux, Y.; de Groot, F. *Actes J. Grand-Est, Strasbourg* **1994**.

(40) Figgis, B. N.; Kucharski, E. S.; Vrtis, M. *J. Am. Chem. Soc.* **1993**, *115*, 176−181.

(41) Siberchicot, B. Private communication.